Multistability, chaos, and random signal generation in semiconductor superlattices

Lei Ying,[1] Danhong Huang,[2,3] and Ying-Cheng Lai[1,4,*]

[1]*School of Electrical, Computer, and Energy Engineering, Arizona State University, Tempe, Arizona 85287, USA*

[2]*Air Force Research Laboratory, Space Vehicles Directorate, Kirtland Air Force Base, New Mexico 87117, USA*

[3]*Center for High Technology Materials, University of New Mexico, 1313 Goddard St. SE, Albuquerque, New Mexico 87106, USA*

[4]*Department of Physics, Arizona State University, Tempe, Arizona 85287, USA*

Historically, semiconductor superlattices, artificial periodic structures of different semiconductor materials, were invented with the purpose of engineering or manipulating the electronic properties of semiconductor devices. A key application lies in generating radiation sources, amplifiers, and detectors in the "unusual" spectral range of subterahertz and terahertz (0.1–10 THz), which cannot be readily realized using conventional radiation sources, the so-called THz gap. Efforts in the past three decades have demonstrated various nonlinear dynamical behaviors including chaos, suggesting the potential to exploit chaos in semiconductor superlattices as random signal sources (e.g., random number generators) in the THz frequency range. We consider a realistic model of hot electrons in semiconductor superlattice, taking into account the induced space charge field. Through a systematic exploration of the phase space we find that, when the system is subject to an external electrical driving of a single frequency, chaos is typically associated with the occurrence of multistability. That is, for a given parameter setting, while there are initial conditions that lead to chaotic trajectories, simultaneously there are other initial conditions that lead to regular motions. Transition to multistability, i.e., the emergence of multistability with chaos as a system parameter passes through a critical point, is found and argued to be abrupt. Multistability thus presents an obstacle to utilizing the superlattice system as a reliable and robust random signal source. However, we demonstrate that, when an additional driving field of incommensurate frequency is applied, multistability can be eliminated, with chaos representing the only possible asymptotic behavior of the system. In such a case, a random initial condition will lead to a trajectory landing in a chaotic attractor with probability 1, making quasiperiodically driven semiconductor superlattices potentially as a reliable device for random signal generation to fill the THz gap. The interplay among noise, multistability, and chaos is also investigated.

I. INTRODUCTION

A semiconductor superlattice consists of a periodic sequence of thin layers of different types of semiconductor materials, which was conceived by Esaki and Tsu [1] with the purpose of engineering the electronic properties of the structure. Specifically, a superlattice is a periodic structure of coupled quantum wells, where at least two types of semiconductor materials with different band gaps are stacked on top of each other along the so-called growth direction in an alternating fashion [2,3]. For a structure consisting of two materials, e.g., GaAs and AlAs, the regions of GaAs serve as quantum wells while those of AlAs are effectively potential barriers. As a result, the conduction band of the whole system exhibits spatially periodic modulation with the period given by the combined width of the quantum well and the barrier, which is typically much larger than the atomic lattice constant. If the widths of the barriers are sufficiently small, then the quantum wells are strongly coupled through the mechanism of quantum tunneling, effectively forming a one-dimensional energy band in the growth direction. Because of the relatively large spatial period of the superlattice as compared with the atomic lattice spacing, the resulting Brillouin zones and the bandwidths are much smaller than the inverse of the atomic lattice constant, leading to a peculiar type of band structure: the miniband. For larger barrier width, the quantum wells are weakly coupled so resonant tunneling of electrons between adjacent wells

occurs and becomes dominantly sequential. When an external voltage (bias) is applied, electronic transport can occur, making superlattice appealing to investigating and exploiting various transport phenomena [4]. More generally, the unique perspective or freedom to design electronic properties makes semiconductor superlattices a paradigm to study many phenomena in condensed matter physics and device engineering [5].

While electronic transport in semiconductor superlattices should be treated quantum mechanically in principle, the presence of an external field and the many-body effect through the electron-electron Coulomb interaction make a full quantum treatment practically impossible. An effective approach to modeling transport dynamics in the superlattice system is through the force-balance equation [6–15], which can be derived either from the classical Boltzmann transport equation [9,10] or from the Heisenberg equation of motion [16,17]. In spite of a quantum system's being fundamentally linear, the self-consistent field caused by the combined effects of the external bias and the intrinsic many-body mean field becomes effectively nonlinear [18,19]. In the high field transport regime, various nonlinear phenomena including chaos can arise [4]. In the past two decades, there were a host of theoretical and computational studies of chaotic dynamics in semiconductor superlattices [4,18–32]. The effects of magnetic field on the nonlinear dynamics in superlattices were also investigated [33–35]. Experimentally, a number of nonlinear dynamical behaviors were observed and characterized [3,36–39].

A key application of semiconductor superlattices is to fill the so-called "THz" gap, i.e., to develop radiation sources,

*Ying-Cheng.Lai@asu.edu

amplifiers, and detectors [40–44] from 0.1 to 10 THz, the frequency range in which convenient radiation sources are not readily available [45–48]. In particular, below 0.1 THz electron-transport-based devices are typical, and above 10 THz devices based on optical transitions (e.g., solid-state lasers) are commonly available. Since, in general, chaotic systems can be used as random number generators [49–57], the ubiquity of chaos in semiconductor superlattices implies that such systems may be exploited for random signal generation in the frequency range corresponding to the THz gap. Motivated by this, in this paper we are led to investigate the dynamics of energetic or "hot" electrons in semiconductor superlattices. Specifically, we study the setting where the system is subject to strong dc and ac fields so miniband conduction occurs effectively in a quasi-one-dimensional superlattice. Due to the strong driving field, a space charge field is induced, which contains two nonlinear terms in the equation of motion. The main issue we address is that of reliability and robustness, i.e., for a given parameter setting, what is the probability to generate chaos from a random initial condition? We find that, for the common case of a single ac driving field, onset of chaos is typically accompanied by the emergence of multistability in the sense that there are coexisting attractors in the phase space which are not chaotic. Using the ensemble method to calculate the maximum Lyapunov exponent, we distinguish the regular from the chaotic attractors. The probability for a random initial condition to lead to chaos is finite but in general is not close to unity. Due to the simultaneous creation of the basin of attraction of the chaotic attractor, the transition to multistability with chaos, as a system parameter passes through a critical point, is necessarily abrupt. Likewise, the disappearance of multistability is abrupt, as the typical scenario for a chaotic attractor to be destroyed is through a boundary crisis [58], which is sudden with respect to parameter variations. From the point of view of random signal generation, multistability is thus undesired. We find, however, that an additional driving field, e.g., of an incommensurate frequency, can effectively eliminate multistability to guarantee the existence of open parameter regions in which the probability of generating chaos from random initial conditions is unity. We also find that, due to multistability, weak noise can suppress chaos but strong noise can lead to chaos with probability 1.

We note that, in nonlinear dynamical systems, multistability is a common phenomenon [59–69]. Earlier works focused on low-dimensional nonlinear dynamical systems with a few [59–63] and many coexisting attractors [64,65]. Recently multistability has been uncovered in nanosystems such as the electrically driven silicon nanowire [56,67] described by nonlinear partial differential equations, as well as in a coupled system of a ferromagnet and a topological insulator [69]. The issue of controlling multistability was also addressed [64,68,70–72]. Multistability was uncovered in semiconductor superlattices as well [73–75]. The multistability phenomenon studied in the present work, however, is associated with the dynamics of hot electrons.

II. MODEL

In weakly coupled superlattices in which sequential resonant tunneling is the main transport mechanism, chaos can

arise and its potential use as a random number generator has been proposed [3,5,22]. In our work, we focus on the strongly coupled regime, in which miniband conduction is the primary contribution to transport.

Using the force-balance equation [76] for an n-doped semiconductor quantum-dot superlattice, we write the dynamical equation for the electron center-of-mass velocity $V_c(t)$ as

$$
\begin{aligned}
\frac{dV_c(t)}{dt} = & -[\gamma_1 + \Gamma_c \sin(\Omega_c t)]V_c(t) \\
& + \frac{e}{M(\mathcal{E}_e)}[E_0 + E_1 \cos(\Omega_1 t) \\
& + E_1' \cos(\Omega_1' t) + E_{sc}(t)],
\end{aligned} \tag{1}
$$

where γ_1 is the momentum-relaxation rate constant; Γ_c comes from channel-conductance modulation with Ω_c being the modulation frequency; $M(\mathcal{E}_e)$ is the energy-dependent averaged effective mass of an electron in the superlattice; $\mathcal{E}_e(t)$ is the average energy per electron; E_0 is the applied dc electric field; E_1 and E_1' are the amplitudes of the two external ac fields with frequencies Ω_1 and Ω_1', respectively; and $E_{sc}(t)$ is the induced space-charge field due to the excitation of plasma oscillation. Here, the statistical resistive force [76] has been approximated by the momentum relaxation rate. Based on the energy-balance equation, one can show [77] that $\mathcal{E}_e(t)$ satisfies the following dynamical equation:

$$
\begin{aligned}
\frac{d\mathcal{E}_e(t)}{dt} = & -\gamma_2[\mathcal{E}_e(t) - \mathcal{E}_0] \\
& + eV_c(t)[E_0 + E_1 \cos(\Omega_1 t) \\
& + E_1' \cos(\Omega_1' t) + E_{sc}(t)],
\end{aligned} \tag{2}
$$

where γ_2 is the energy-relaxation rate constant and $\mathcal{E}_0$ is the average electron energy at the thermal equilibrium, and the thermal energy exchange of the electrons with the crystal lattice [77] is approximately described by the γ_2 term. Applying the Kirchoff's theorem to a resistively shunted quantum-dot superlattice [18], we obtain [78] the dynamical equation for the induced space-charge field $E_{sc}(t)$ as

$$
\frac{dE_{sc}(t)}{dt} = -\gamma_3 E_{sc}(t) - \left(\frac{en_0}{\epsilon_0 \epsilon_b}\right)V_c(t), \tag{3}
$$

where γ_3, which is inversely proportional to the product of the system resistance and the quantum capacitance, is the dielectric relaxation rate constant [78], n_0 is the electron concentration at the thermal equilibrium, and ϵ_b is the relative dielectric constant of the host semiconductor material. The exact microscopic calculations of γ_1 and γ_2 in the absence of space-charge field were carried out previously [79] based on the semiclassical Boltzmann transport equation and the coupled force-energy balance equations [25], respectively. Equivalent quantum calculations of γ_1 and γ_2 can also be done through the coupled force balance and the Boltzmann scattering equations [76]. The space charge field is the sole source of nonlinearity.

Within the tight-binding model, the single-electron kinetic energy ε_k in a semiconductor quantum-dot superlattice can be written as

$$
\varepsilon_k = \frac{\Delta}{2}[1 - \cos(kd)], \tag{4}
$$

where k ($|k| \leqslant \pi/d$) is the electron wave number along the superlattice growth direction, Δ is the miniband width, and d is the spatial period of the superlattice. This energy dispersion relation gives [76]

$$\frac{1}{M(\mathcal{E}_\mathrm{e})} = \left\langle \frac{1}{\hbar^2} \frac{d^2 \varepsilon_k}{dk^2} \right\rangle = \frac{1}{m^*} \left[1 - \left(\frac{2}{\Delta} \right) \mathcal{E}_\mathrm{e}(t) \right], \quad (5)$$

where $m^* = 2\hbar^2/\Delta d^2$ and $|1/M(\mathcal{E}_\mathrm{e})| \leqslant 1/m^*$.

For numerical calculations, it is convenient to use dimensionless quantities. Specifically, we introduce $v(\tau) = (m^* d/\hbar) V_\mathrm{c}$, $w(\tau) = [(2/\Delta)\mathcal{E}_\mathrm{e} - 1]$, $f(\tau) = (ed/\hbar\omega_0) E_\mathrm{sc}$, and $\tau = \omega_0 t$ with $\omega_0 = 1$ THz being the frequency scale. In terms of the dimensionless quantities, the dynamical equations of the resonantly tunneling electrons in the superlattice become

$$\frac{dv(\tau)}{d\tau} = -b_1 v(\tau)[1 + a_2 \sin(\bar{\Omega}\tau)]$$
$$\quad - [a_0 + a_1 \cos(\Omega\tau) + a_1' \cos(\Omega'\tau) + f(\tau)]w(\tau),$$
$$\frac{dw(\tau)}{d\tau} = -b_2[w(\tau) - \overline{w}_0]$$
$$\quad + [a_0 + a_1 \cos(\Omega\tau) + a_1' \cos(\Omega'\tau) + f(\tau)]v(\tau),$$
$$\frac{df(\tau)}{d\tau} = -b_3 f(\tau) - a_3 v(\tau), \quad (6)$$

where $\overline{w}_0 = [(2/\Delta)\mathcal{E}_0 - 1] = -1$, $b_1 = \gamma_1/\omega_0$, $b_2 = \gamma_2/\omega_0$, $b_3 = \gamma_3/\omega_0$, $a_0 = \omega_\mathrm{B}/\omega_0$, $a_1 = \omega_\mathrm{s}/\omega_0$, $a_1' = \omega_\mathrm{s}'/\omega_0$, $a_2 = \Gamma_\mathrm{c}/\gamma_1$, and $a_3 = (\Omega_\mathrm{c}/\omega_0)^2$ are all positive real constants. The field related parameters are $\omega_\mathrm{B} = eE_0 d/\hbar$, $\omega_\mathrm{s} = eE_1 d/\hbar$, $\omega_\mathrm{s}' = eE_1' d/\hbar$, $\Omega = \Omega_1/\omega_0$, $\Omega' = \Omega_1'/\omega_0$, $\bar{\Omega} = \Omega_\mathrm{c}/\omega_0$, and $\Omega_c = \sqrt{e^2 n_0/m^* \epsilon_0 \epsilon_\mathrm{b}}$, where the last quantity is the bulk plasma frequency. The fields are assumed to be turned on at $t = 0$. The initial conditions for Eq. (6) are $v(0) = v_0, f(0) = f_0$, and $w(0) = w_0$.

III. RESULTS

A. Evidence of multistability

In the absence of the space-charge field $E_\mathrm{sc}(t)$ from the plasmon excitation, Eqs. (1) and (2) become linearly coupled equations. In such a case, the electron dynamics can be solved exactly [79] by using the semiclassical Boltzmann transport equation subject to a strong dc+ac field, where there is an interplay between the phenomena of Bloch oscillations and dynamical localization, which play an important role in the transport dynamics. When the space charge field $E_\mathrm{sc}(t)$ was included, the motions of the hot electrons in the quantum-dot

superlattice can exhibit chaotic behaviors [18]. The relaxation rates in Eqs. (1) and (2), γ_1 and γ_2, can be evaluated using the coupled force-energy balance equations [25], where the two-dimensional phase diagram of the driving amplitude and frequency in the absence of the dc field, as well as their dependence on the lattice temperature, were computed and analyzed.

The dimensionless Eq. (6) represents a nonlinear dynamical system with $f(\tau)w(\tau)$ and $f(\tau)v(\tau)$ as the specific nonlinear terms. While, in principle, all system parameters can be adjusted, experimentally, certain parameters are not readily susceptible to changes, especially those characterizing the material properties such as $\gamma_{1,2,3}$. Adjustable are the parameters associated with the driving dc or ac electric field such as a_0, a_1, a_1' and the frequencies Ω and Ω'.

To search for multistability, we use the method of ensemble simulations by which we choose a large number of random initial conditions and determine the asymptotic state for each initial condition. As shown schematically in Fig. 1(a), under the same parameter setting, two initial conditions can lead to two completely different attractors, one regular and another chaotic. For better visualization of the basins of the distinct attractors, we select a number of parallel planes in the dynamical variables (v, w) for a set of systematically varying values of the third variable f. Figure 1(b) shows, for $a_1 = 1.9$ ($E_1 < E_0$), the basin structures of 11 such planes, where we find two final states: one steady-state (blue) and another chaotic (yellow) attractors. A general feature is that the basin structures appear quite irregular, and there are approximately equal numbers of initial conditions that lead to each of the two distinct attractors. As the amplitude of the modulated field is increased to $a_1 = 2.3$ ($E_1 > E_0$), the number of initial conditions that lead to the chaotic attractor is apparently more than that to the steady-state attractor, as shown in Fig. 1(c). In both Figs. 1(b) and 1(c), for $f_0 > 0$ there is an open area near $(v_0, w_0) = (0, 0)$ which belongs to the basin of the chaotic attractor, indicating a high probability for the system trajectory to land in this attractor and henceforth ubiquity of chaos associated with hot electron motions in the superlattice. Representative examples of the evolution towards a chaotic attractor are shown in Figs. 2(a)–2(d).

B. Abrupt transition to multistability with chaos

To determine the nature of the distinct asymptotic attractors of the system, we use the standard maximum (nontrivial) Lyapunov exponent λ_m, where a positive and a negative value indicates a chaotic and a regular attractor, respectively. The time-dependent Jacobian matrix of Eq. (6) is

$$\mathcal{A}(\tau) = \begin{pmatrix} -b_1[1 + a_2 \sin(\bar{\Omega}\tau)] & -a_0 + a_1 \cos(\Omega\tau) + a_1' \cos(\Omega'\tau) + f(\tau) & -w(\tau) \\ a_0 + a_1 \cos(\Omega\tau) + a_1' \cos(\Omega'\tau) + f(\tau) & -b_2 & v(\tau) \\ -a_3 & 0 & -b_3 \end{pmatrix}. \quad (7)$$

The maximum Lyapunov exponent can be calculated through

$$\frac{d\mathbf{x}(\tau)}{d\tau} = \mathcal{A}(\tau) \cdot \mathbf{x}(\tau), \quad (8)$$

where $\mathbf{x}$ is a unit tangent vector.

Statistically, what is the route to chaos for hot electron motion in the superlattice as a system (bifurcation) parameter is changed, and how likely is multistability? From the standpoint of relative basin volumes, the transition must be abrupt
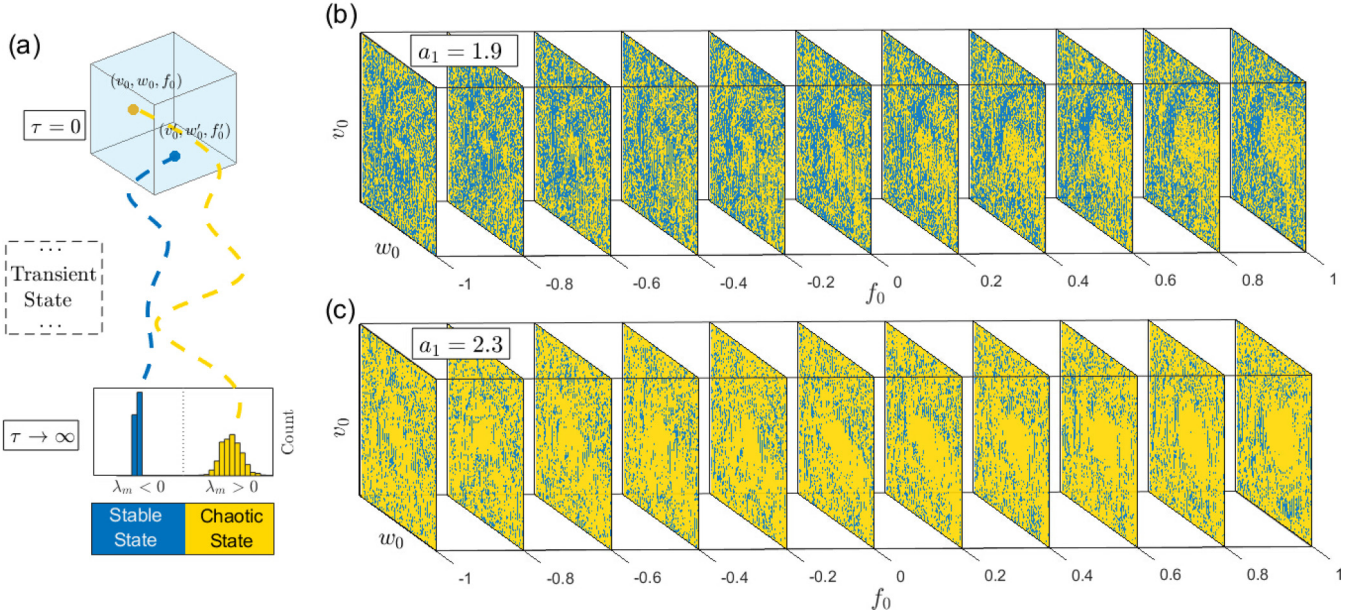
FIG. 1. Evidence of multistability: Multiple coexisting attractors and their basins of attraction. (a) Schematic diagram of multistability resulting from different choices of the initial conditions v_0, w_0, and f_0. Two distinct sets of initial conditions, (v_0, w_0, f_0) and (v_0', w_0', f_0'), chosen from a cube in the (v, w, f) space, can result in a stable steady state and chaos, respectively. The dashed blue and yellow traces signify that the asymptotic state is a regular steady-state (blue) and a chaotic attractor (yellow), respectively, as indicated by the distribution of the maximum Lyapunov exponent calculated from a large number of initial conditions. [(b) and (c)] Basins of attraction of the steady-state and the chaotic attractors in the (v_0, w_0) plane for a systematically varying set of values of f_0 (for $f_0 \in [-1, 1]$ in increments of 0.2) for $a_1 = 1.9$ and $a_1 = 2.3$, respectively. The ranges of v_0 and w_0 are $|v_0| \leqslant 1$ and $|w_0| \leqslant 1$. Other parameters for both (b) and (c) are $a_0 = 2.23, a_1' = a_2 = 0$, $a_3 = 7.48, b_1 = 0.28, b_2 = b_3 = 2.85 \times 10^{-2}$, and $\Omega = 1.34$.
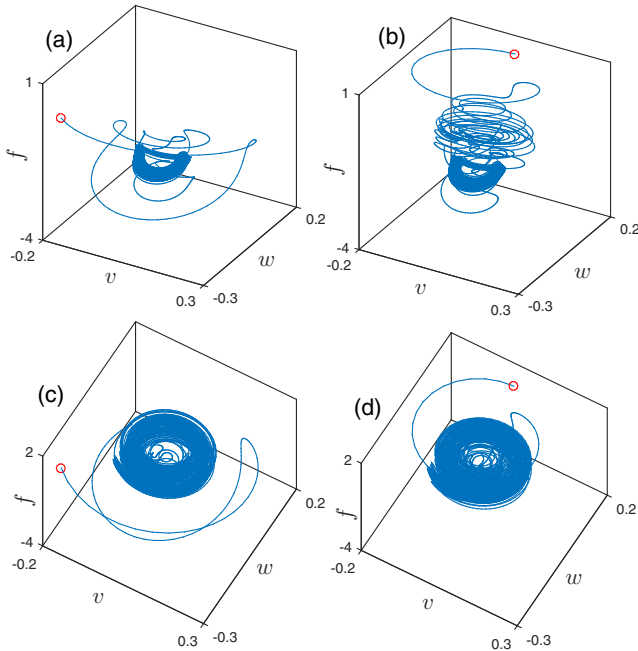

FIG. 2. Examples of chaotic dynamics associated with multistability. [(a)–(d)] Four representative trajectories evolving toward a chaotic attractor in the three-dimensional phase space. The initial conditions are $(v_0, w_0, f_0) = (-0.2, -0.2, -0.6)$ for panels (a) and (c) and $(0, 0.2, 0.4)$ for panels (b) and (d). The value of the bifurcation parameter is $a_1 = 1.9$ for (a) and (b) and $a_1 = 2.3$ for (c) and (d). Other parameters are $a_0 = 2.23, a_1' = a_2 = 0, a_3 = 7.48, b_1 = 0.28$, $b_2 = b_3 = 2.85 \times 10^{-2}$, and $\Omega = 1.34$.

because, when a chaotic attractor emerges (e.g., through the standard period doubling route [80]), its basin is created simultaneously. Thus, if we calculate the probability for a random trajectory to land in the chaotic attractor versus the bifurcation parameter, we expect to see an abrupt increase in the probability from zero to a finite value as the parameter passes through a critical point. This has indeed been found in the superlattice system, as shown in Figs. 3(a) and 3(c) for fixed $a_0 = 2.23$ and a_1 increasing systematically from 1.0 to 3.0. Specifically, shown in Fig. 3(a) are the values of the maximum Lyapunov exponent λ_m versus a_1 from a large number of random initial conditions chosen from a unit cube $|v_0, w_0, f_0| < 1$ in the phase space. Figure 3(b) shows the probability of having $\lambda_m > 0$ versus a_1. For $a_1 \approx 1.65$, we observe an abrupt increase in the probability of having chaos. Similarly, disappearance of chaos (e.g., through the typical mechanism of boundary crisis [58]) must also be abrupt because, as a chaotic attractor is destroyed, its basin disappears simultaneously as it is absorbed into the basin of the coexisting regular attractor. This behavior occurs for $a_1 \approx 2.45$, as shown in Fig. 3(c). Since the probability of having chaos is never unity, we see that multistability arises for $1.65 \lesssim a_1 \lesssim 2.45$ (except for the values of a_1 corresponding to the occurrence of periodic windows), in which a chaotic and a regular attractors coexist.

Abrupt emergence and disappearance of multistability associated with chaos also occur for fixed $a_1 = 2.13$ and varying a_0, as shown in Figs. 3(b) and 3(d). We see that the maximum probability of landing in a chaotic attractor is relatively small as compared with that for Figs. 3(c). Even if the
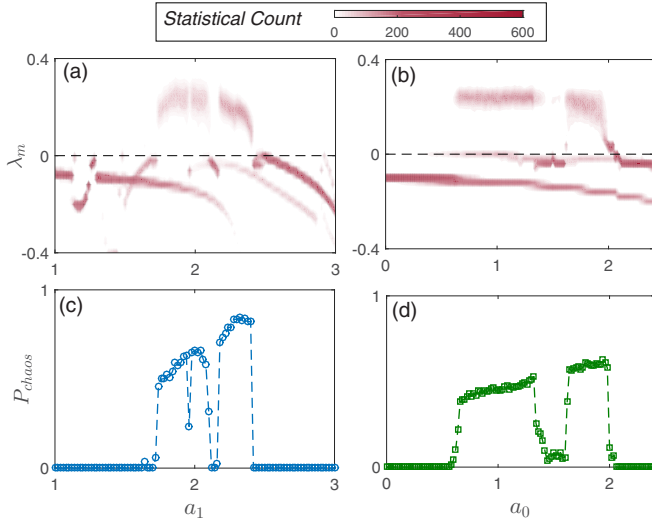
FIG. 3. Transition to chaos and multistability. (a) For fixed $a_0 = 2.23$, the values of the maximum Lyapunov exponent λ_m calculated from an ensemble of initial conditions versus a_1 for $1.0 \leqslant a_1 \leqslant 3.0$. (b) A similar plot but for fixed $a_1 = 2.13$ and a_0 varying in the range [1.0,2.4]. (c) For $a_0 = 2.23$, the probability versus a_1 for a random trajectory to land in a chaotic attractor. (d) A plot similar to that in (c) but for fixed $a_1 = 2.13$ and varying a_0. Other parameters are $a'_1 = a_2 = 0$, $a_3 = 7.48$, $b_1 = 0.28$, $b_2 = b_3 = 2.85 \times 10^{-2}$, and $\Omega = 1.34$. From (a) and (c), abrupt emergence of chaos at $a_1 \approx 1.65$ and abrupt disappearance of chaos at $a_1 \approx 2.45$ can be seen (see text for the reason of the "abruptness"). The dips in the probability curve of chaos at $a_1 \approx 2.0$ and $a_1 \approx 2.15$ are due to periodic windows. Abrupt emergence and disappearance of multistability associated with chaos also occur for fixed $a_1 = 2.13$ and varying a_0, as shown in (b) and (d).

system has settled into chaotic motion, due to multistability external disturbances can "push" it out of chaos, which is undesired for random signal generation.

C. Reliable and robust chaos with quasiperiodically driving fields and the effect of noise

The simultaneous emergence of chaos and multistability presents a difficulty in exploiting semiconductor superlattices for applications in random signal generation, a task that requires reliable, robust, and persistent chaotic behaviors. However, due to the coexisting nonchaotic attractor, there is a finite probability that a randomly chosen initial condition would not lead to a chaotic trajectory. Even when the system has settled into a chaotic attractor, random disturbances can drive it out of chaos. Through extensive simulations, we find that, if the system is under a single ac driving, then it is unlikely that the probability of having chaos can reach unity in any open interval. However, we find a relatively simple, experimentally feasible way to eliminate multistability in such a way that the only attractor in the system is chaotic. In particular, when the system is subject to a second ac driving field of incommensurate frequency, transition to chaos can be achieved but without the occurrence of multistability.

Figures 4(a) and 4(b) demonstrate the occurrence of chaos with probability 1 when the superlattice system is under
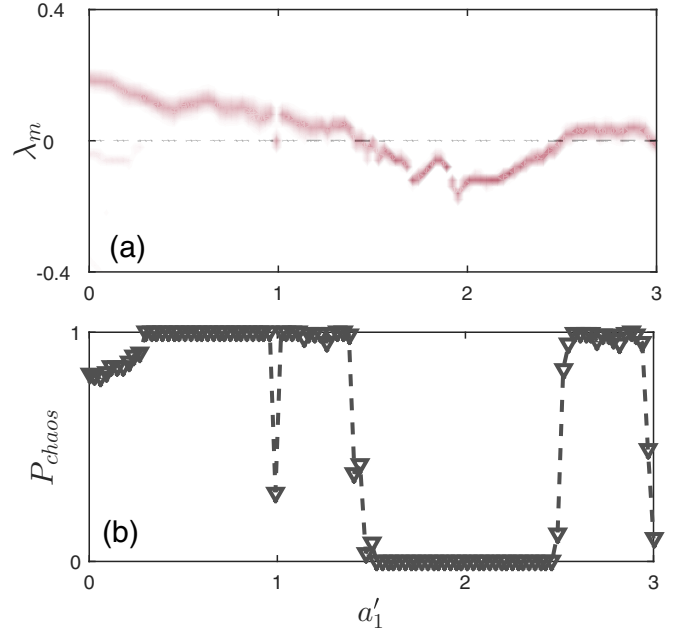

FIG. 4. Occurrence of reliable and robust chaos with probability 1 under quasiperiodic driving. When a second ac driving field of amplitude a'_1 and frequency $\Omega' = \sqrt{2}$ is applied to the superlattice system, open parameter intervals emerge in which the probability of generating chaos from a random initial condition is unity. (a) Statistical counts of the maximum Lyapunov exponent and (b) probability of generating chaos versus a'_1. Other parameters are $a_0 = 2.23$, $a_1 = 2.3$, $a_2 = 0$, $a_3 = 7.48$, $b_1 = 0.28$, $b_2 = b_3 = 2.85 \times 10^{-2}$, and $\Omega = 1.34$.

quasiperiodic driving, i.e., when a second ac driving field, $a'_1 \cos(\Omega' \tau)$, is present for $\Omega' = \sqrt{2}$. In particular, Fig. 4(a) shows, for systematically varying amplitude a'_1, the possible values of the maximum Lyapunov exponent where, for each fixed value of a'_1, the distinct values of the exponent from a large number of initial conditions are displayed. Figure 4(b) shows the probability of generating chaos versus the driving amplitude a'_1, where we see that there are open parameter intervals in which the probability is 1. Thus, in spite of the periodic windows, in these open intervals the only attractor of the system is chaotic, effectively eliminating multistability. Due to the openness of the parameter intervals for chaos, generic perturbation will not drive the system out of chaos, making it suitable for random signal generation. Figure 5(a) presents an example of the statistical distribution of the values associated with a typical chaotic signal, which is approximately Gaussian. Figure 5(b) shows the autocorrelation of the signal, which exhibits a desired decaying behavior.

In weakly coupled systems [81,82], noise can induce chaos. We find, however, that in strongly coupled systems, noise, depending on its amplitude, can either suppress or enhance chaos. In particular, due to multistability, weak noise tends to "kick" a chaotic trajectory out of its basin of attraction and drives the system to the coexisting regular attractor. If noise is sufficiently strong, then the system can be driven out of the basin of the regular attractor towards the chaotic attractor. In either case, multistability is destroyed, as under noise there is only a single attractor that can be either regular or
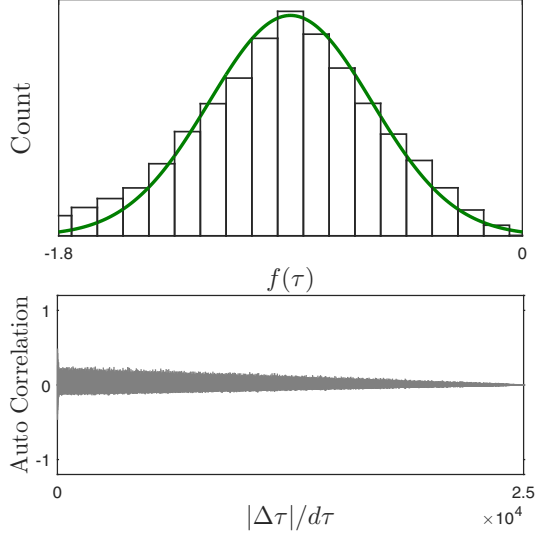
FIG. 5. Statistical properties of chaos for random signal generation. Under quasiperiodic driving ($\Omega = 1.34$ and $\Omega' = \sqrt{2}$), (a) distribution of the values of a chaotic time series $f(\tau)$. The green dashed curve is a fitted Gaussian with mean $\mu = -0.9$ and variance $\sigma^2 = 0.1$. (b) Autocorrelation of the chaotic time series, where $\Delta\tau$ is the time difference $\tau - \tau'$ and $d\tau$ is the time step used in the numerical integration of the equations of motion. Other parameters are identical to those in Fig. 4.
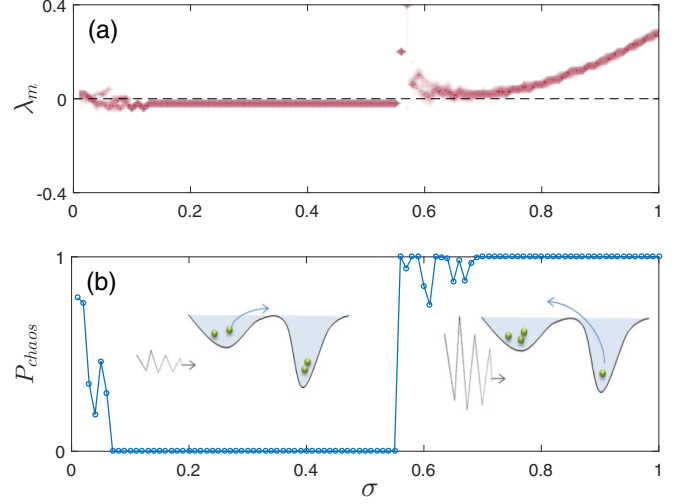

FIG. 6. Effect of noise on multistability and chaos. When noise of zero mean is applied to the voltage driving, for weak noise chaos is suppressed but it is enhanced for strong noise. In the latter case there are open parameter intervals in which the probability of generating chaos from a random initial condition is unity. (a) Statistical counts of the maximum Lyapunov exponent and (b) probability of generating chaos versus a'_1. Other parameters are the same as for Fig. 4 except $a'_1 = 0$. A simple mechanical system illustrating the interplay among noise, multistability, and chaos is included in (b); see text for details.

chaotic depending on the noise amplitude. To demonstrate this phenomenon, we apply uncorrelated noise $a_0 \to a_0 + a^{in}(t)$ with a Gaussian distribution to the voltage driving, where $\langle a^{in}(t)a^{in}(t')\rangle = \sigma^2\delta(t - t')$. We find, for $0.06 \lesssim \sigma \lesssim 0.56$ (the weak-noise regime for the particular parameter setting), that the stable steady state is the only attractor in the system as noise can drive a chaotic trajectory into the stable steady-state attractor. In contrast, in the strong-noise regime ($\sigma \gtrsim 0.56$), the chaotic attractor is the only attractor in the system. The phenomena can be intuitively illustrated using a simple mechanical system in which a particle moves in an asymmetrical double potential well system. As indicated in Fig. 6(b), the stable steady-state and the chaotic attractors are represented by the deep and shallow wells, respectively. Weak noise can drive the particle from the shallow well and kick it into the deep well with a lower energy, but the opposite cannot occur due to the weakness of noise and the well depth. However, for strong noise, the random energy can be sufficient to excite particle out of the deep well. We remark that noise-induced chaos is a well-documented phenomenon in nonlinear dynamics (see, for example, Refs. [83–88]).

D. Physical mechanism of chaos and multistability

The physical mechanism for the evolution of the basin structure toward a more chaos dominated one [Fig. 1(c)] as the ac driving amplitude is increased can be understood as follows. From Eq. (1), we find that the quantity $1/M(\mathcal{E}_e)$ controls the switching between the in-phase (acceleration with $dV_c/dt > 0$) and the out-of phase (deceleration with $dV_c/dt < 0$) electron motions with respect to the driving dc+ac field. Equation (2) also indicates that the in-phase and

out-of phase motions are associated with the increase (field-power absorption) and decrease (field-power amplification) in the average electron energy $\mathcal{E}_e$ ($\geqslant 0$). A change in $\mathcal{E}_e$ directly leads to $M(\mathcal{E}_e) > 0$ for $0 \leqslant \mathcal{E}_e < \Delta/2$ or $M(\mathcal{E}_e) < 0$ for $\Delta/2 < \mathcal{E}_e \leqslant \Delta$. This gives rise to an upper limit for the velocity amplitude $|V_c|$.

In the absence of the ac field, by neglecting decays and the space-charge field, we get from Eqs. (1) and (2)

$$\frac{d^2 V_c(t)}{dt^2} + \omega_B^2 V_c(t) = 0, \qquad (9)$$

where $\omega_B = eE_0 d/\hbar$ is the Bloch frequency. The dc field can thus drive the electrons into periodic Bloch oscillations with the frequency $\omega = \omega_B$ due to the periodic superlattice band structure. In the presence of an external ac field, the combination of the $E_1 \cos(\Omega_1 t)\mathcal{E}_e(t)$ term in Eq. (1) and the $E_1 \cos(\Omega_1 t)V_c(t)$ term in Eq. (2) will generate many harmonic ac fields in the system. Specifically, including the primary ac field but still neglecting decays and the space-charge field in Eqs. (1) and (2), we obtain its nth harmonics in the oscillating $V_c(t)$ with the frequency $\omega = n\Omega_1$ and the amplitude $|V_c| \sim (eE_1 d/\hbar\Omega_1)^{2n-1}/(2n - 1)!!$, where $n = 2, 3, \ldots$. These harmonic ac fields interact with the electron Bloch oscillations by forming multiple resonances at $\omega = \omega_B \pm n\Omega_1$. Note that, without any harmonics, the system dynamics is similar to that of a forced pendulum, which can typically have chaotic motion for large driving amplitude and low frequency. For small values of E_1, i.e., $(eE_1 d/\hbar\Omega_1) < 1$, we anticipate only a few periodic oscillating modes associated with the isolated multiresonances, which manifest themselves as islands (or gaps) in the E_1-Ω_1 plane. As the driving force is increased ($E_1 > E_0$) and the driving frequency is decreased

($\Omega_1 < \Omega_B$), a large number of enhanced harmonic ac modes emerge in the system for $(eE_1d/\hbar\Omega_1) > 1$. In such a case, the multiple resonance-induced islands in the E_1-Ω_1 phase space are widened and become overlapped. As a result, the electron motion switches from a periodic-dominant pattern to a chaotic-dominant one.

Equation (3) contains a self-consistent oscillating space-charge field $E_{sc}(t)$, whose amplitude $|E_{sc}|$ tends to grow with the amplitude $|V_c|$ of the electron velocity. From the combination of the $E_{sc}(t)\mathcal{E}_e(t)$ term in Eq. (1) and the $E_{sc}(t)V_c(t)$ term in Eq. (2), we expect much higher harmonics of the primary ac field to develop rapidly in the system insofar as $(eE_1d/\hbar\Omega_1) \gtrsim 1$. In fact, a straightforward calculation indicates $|E_{sc}| \sim (eE_1d/\hbar\Omega_1)^{\alpha_n}$, where the sequence $\alpha_n = 2\alpha_{n-1} + \alpha_{n-2}$ with $\alpha_1 = 1$ and $\alpha_2 = 3$ diverges fast with n [i.e., $\lim_{n\to\infty}(\alpha_n/\alpha_{n-1}) = 1 + \sqrt{2}$]. In short, by including the self-consistent oscillating space-charge field, the superlattice system will be driven quickly into a chaotic regime insofar as Ω_c/Ω_1 is large and the condition $eE_1d/\hbar\Omega_1 > 1$ is met.

We remark that, in the miniband approach, the balance equation [Eq. (1)] is valid only if the electric field in the superlattice is homogeneous. With such an electric field, the system dynamics is generally unstable when the dc differential conductivity is negative—the so-called NDC instability [13,30]. The normalized dc current density j_{dc}^{Ω}/j_p in the superlattice can be estimated using the Esaki-Tsu characteristic and the Tucker relations [5,89–93]. For the static case with only dc driving field a_0, the parameters in our simulation are located in the NDC instability regime. However, with an ac driving, transport can be enhanced by a quantized energy ("photon") caused by the ac field. As a result, the differential conductivity is not always negative for large values of a_0 [94,95]. The differential conductivity becomes positive for $a_0 = n\Omega$, where $n = 1,2,\dots$. Using the same parameter setting as in Figs. 3(b) and 3(d), we find that, near $a_0 = 1\Omega \approx 1.34$, the regime of chaos (gray regime in Fig. 7) covers completely the positive differential conductivity regime, indicating the existence of parameter regimes of chaos but without the NDC instability and, as such, the NDC instability may not be a contributing factor to chaos. Indeed, since our model is based on a single miniband, it pre-excludes any NDC effect. In addition, the field domain effect is expected to be small if the period of the superlattice is short and the number of periods is not too large. A complete analysis of the NDC instability and its possible interplay with chaotic dynamics is beyond the scope of the present work.

IV. DISCUSSION

Semiconductor superlattices, due to their potential applications as radiation sources, amplifiers, and detectors in the THz spectral range, have been extensively studied. There has also been a great deal of effort in investigating nonlinear
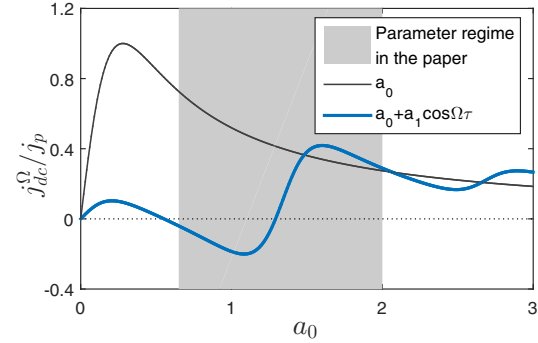

FIG. 7. IV curve for the superlattice system. The black thin and blue thick curves are calculated based on the Esaki-Tsu characteristic and the Tucker relation. The gray domain denotes the parameter regime in our study.

dynamics in superlattice systems. Especially, chaos has been demonstrated as a generic behavior, suggesting the possibility of random signal generation in the THz range. For such applications it is desired that chaos be reliable and robust in the sense that disturbances to the system shall not drive it out of chaos. In spite of the previous works in this field, the issues have not been addressed of whether chaos in semiconductor superlattice is reliable and robust and, if not, what can be done to overcome the difficulty.

The main result of our work is demonstration that, for energetic electrons in semiconductor superlattices subject to an external periodic driving field, chaos and multistability go side by side in the sense that they emerge and disappear simultaneously as a system parameter is changed. Due to the creation of the basin of attraction associated with the birth of a chaotic attractor, the transition to multistability is necessarily abrupt. As a result of multistability, for any given parameter the probability of generating chaos from a random initial condition will in general not be close to unity. We develop a heuristic physical understanding for the emergence of chaos and multistability. To eliminate multistability and ensure that chaos is the only outcome for any random initial condition, we find that the approach of applying quasiperiodic ac driving can be effective. Experimentally, it may be feasible to apply a second ac electric field to drive the superlattice system. Our work demonstrates that robust chaos can emerge, making semiconductor superlattice with quasiperiodic driving a potential candidate for random signal generation in the THz range.

[1] L. Esaki and R. Tsu, IBM J. Res. Dev. **14**, 61 (1970).

[2] H. T. Grahn, *Semiconductor Supperlattices, Growth and Electronic Properties* (World Scientific, Singapore, 1995).

[3] Y. Zhang, J. Kastrup, R. Klann, K. H. Ploog, and H. T. Grahn, Phys. Rev. Lett. **77**, 3001 (1996).

[4] E. Schöll, *Nonlinear Spatiotemporal Dynamics and Chaos in Semiconductors* (Cambridge University Press, Cambridge, UK, 2001).

[5] A. Wacker, Phys. Rep. **357**, 1 (2002).

[6] X. L. Lei and C. S. Ting, Phys. Rev. B **30**, 4809 (1984).

[7] X. L. Lei and C. S. Ting, Phys. Rev. B **32**, 1112 (1985).

[8] X. L. Lei, N. J. M. Horing, and H. L. Cui, Phys. Rev. Lett. **66**, 3277 (1991).

[9] X. L. Lei, J. Phys. Cond. Matt. **6**, 10043 (1994).

[10] X. L. Lei, J. Phys. Cond. Matt. **6**, 9189 (1994).

[11] A. A. Ignatov, E. P. Dodin, and V. I. Shashkin, Mod. Phys. Lett. B **5**, 1087 (1991).

[12] R. R. Gerhardts, Phys. Rev. B **48**, 9178 (1993).

[13] M. Büttiker and H. Thomas, Phys. Rev. Lett. **38**, 78 (1977).

[14] M. Büttiker and H. Thomas, Z. Phys. B **33**, 275 (1979).

[15] M. Büttiker and H. Thomas, Z. Phys. B **34**, 301 (1979).

[16] X. L. Lei, Phys. Status Solidi B **170**, 519 (1992).

[17] X. L. Lei, J. Phys.: Condens. Matter **7**, L429 (1995).

[18] K. N. Alekseev, E. H. Cannon, J. C. McKinney, F. V. Kusmartsev, and D. K. Campbell, Phys. Rev. Lett. **80**, 2669 (1998).

[19] K. N. Alekseev, G. P. Berman, D. K. Campbell, E. H. Cannon, and M. C. Cargo, Phys. Rev. B **54**, 10625 (1996).

[20] O. M. Bulashenko, M. J. García, and L. L. Bonilla, Phys. Rev. B **53**, 10008 (1996).

[21] M. Patra, G. Schwarz, and E. Schöll, Phys. Rev. B **57**, 1824 (1998).

[22] K. J. Luo, H. T. Grahn, K. H. Ploog, and L. L. Bonilla, Phys. Rev. Lett. **81**, 1290 (1998).

[23] K. N. Alekseev, E. H. Cannon, J. C. McKinney, F. V. Kusmartsev, and D. K. Campbell, Physica D **113**, 129 (1998).

[24] J. C. Cao and X. L. Lei, Phys. Rev. B **60**, 1871 (1999).

[25] J. C. Cao, H. C. Liu, and X. L. Lei, Phys. Rev. B **61**, 5546 (2000).

[26] D. Sánchez, G. Platero, and L. L. Bonilla, Phys. Rev. B **63**, 201306 (2001).

[27] K. N. Alekseev and F. V. Kusmartsev, Phys. Lett. A **305**, 281 (2002).

[28] K. N. Alekseev, G. P. Bermana, and D. K. Campbell, Phys. Lett. A **193**, 54 (1994).

[29] A. Amann, J. Schlesner, A. Wacker, and E. Schöll, Phys. Rev. B **65**, 193313 (2002).

[30] L. L. Bonilla and H. T. Grahn, Rep. Prog. Phys. **68**, 577 (2005).

[31] J. Galán, L. L. Bonilla, and M. Moscoso, SIAM J. Appl. Math. **60**, 2029 (2006).

[32] M. T. Greenaway, A. G. Balanov, E. Schöll, and T. M. Fromhold, Phys. Rev. B **80**, 205318 (2009).

[33] S. P. Stapleton, S. Bujkiewicz, T. M. Fromhold, P. B. Wilkinson, A. Patané, L. Eaves, A. A. Krokhin, M. Henini, N. S. Sankeshwar, and F. W. Sheard, Physica D **199**, 166 (2004).

[34] C. Wang and J.-C. Cao, Chaos **15**, 013111 (2005).

[35] A. G. Balanov, D. Fowler, A. Patané, L. Eaves, and T. M. Fromhold, Phys. Rev. E **77**, 026209 (2008).

[36] K. J. Luo, H. T. Grahn, S. W. Teitsworth, and K. H. Ploog, Phys. Rev. B **58**, 12613 (1998).

[37] Y.-H. Zhang, R. Klann, H. T. Grahn, and K. H. Ploog, Superlatt. Microstruc. **21**, 565 (1997).

[38] T. M. Fromhold, A. Patané, S. Bujkiewicz, P. B. Wilkinson, D. Fowler, D. Sherwood, S. P. Stapleton, A. A. Krokhin, L. Eaves, M. Henini, N. S. Sankeshwar, and F. W. Sheard, Nature (London) **428**, 726 (2004).

[39] A. E. Hramov, V. V. Makarov, A. A. Koronovskii, S. A. Kurkin, M. B. Gaifullin, N. V. Alexeeva, K. N. Alekseev, M. T. Greenaway, T. M. Fromhold, A. Patané, F. V. Kusmartsev, V. A. Maksimenko, O. I. Moskalenko, and A. G. Balanov, Phys. Rev. Lett. **112**, 116603 (2014).

[40] T. Hyart, A. V. Shorokhov, and K. N. Alekseev, Phys. Rev. Lett. **98**, 220404 (2007).

[41] T. Hyart, K. N. Alekseev, and E. V. Thuneberg, Phys. Rev. B **77**, 165330 (2008).

[42] T. Hyart, N. V. Alexeeva, J. Mattas, and K. N. Alekseev, Phys. Rev. Lett. **102**, 140405 (2009).

[43] T. Hyart, J. Mattas, and K. N. Alekseev, Phys. Rev. Lett. **103**, 117401 (2009).

[44] T. Hyart, Tunable Superlattice Amplifiers Based on Dynamics of Miniband Electrons in Electric and Magnetic Fields. Ph.D. thesis, University of Oulu, Finland (2009).

[45] P. H. Siegel, IEEE Trans. Microwave Theory Tech. **50**, 910 (2002).

[46] B. Ferguson and X.-C. Zhang, Nat. Mater. **1**, 26 (2002).

[47] T. W. Crowe, W. L. Bishop, D. W. Porterfield, J. L. Hesler, and R. M. Weikle, IEEE J. Solid-State Cir. **40**, 2104 (2005).

[48] M. Tonouchi, Nat. Photon. **1**, 97 (2009).

[49] L. Kocarev, IEEE Cir. Sys. Magaz. **1**, 6 (2001).

[50] T. Stojanovski and L. Kocarev, IEEE Trans. Cir. Sys. I. Fundam. Theor. Appl. **48**, 281 (2001).

[51] T. Stojanovski,, J. Pihl, and L. Kocarev, IEEE Trans. Cir. Sys. I. Fundam. Theor. Appl. **48**, 382 (2001).

[52] M. Drutarovský and P. Galajda, J. Elec. Eng. **57**, 218 (2006).

[53] T. Lin and L. O. Chua, Int. J. Cir. Theo. App. **21**, 473 (2006).

[54] A. Uchida1, K. Amano, M. Inoue, K. Hirano, S. Naito, H. Someya, I. Oowada, T. Kurashige, M. Shiki, S. Yoshimori, K. Yoshimura, and P. Davis, Nat. Photon. **2**, 728 (2008).

[55] I. Reidler, Y. Aviad, M. Rosenbluh, and I. Kanter, Phys. Rev. Lett. **103**, 024102 (2009).

[56] Q. Chen, L. Huang, Y.-C. Lai, C. Grebogi, and D. Dietz, Nano Lett. **10**, 406 (2010).

[57] J.-Z. Zhang, Y.-C. Wang, M. Liu, L.-G. Xue, P. Li, A.-B. Wang, and M.-J. Zhang, Opt. Expr. **20**, 7496 (2012).

[58] C. Grebogi, E. Ott, and J. A. Yorke, Physica D **7**, 181 (1983).

[59] C. Grebogi, S. W. McDonald, E. Ott, and J. A. Yorke, Phys. Lett. A **99**, 415 (1983).

[60] S. W. McDonald, C. Grebogi, E. Ott, and J. A. Yorke, Physica D **17**, 125 (1985).

[61] Y.-C. Lai and C. Grebogi, Phys. Rev. E **52**, R3313 (1995).

[62] Y.-C. Lai, C. Grebogi, J. A. Yorke, and S. C. Venkataramani, Phys. Rev. Lett. **77**, 55 (1996).

[63] Y.-C. Lai and C. Grebogi, Phys. Rev. Lett. **77**, 5047 (1996).

[64] U. Feudel and C. Grebogi, Chaos **7**, 597 (1997).

[65] U. Feudel and C. Grebogi, Phys. Rev. Lett. **91**, 134102 (2003).

[66] Y.-C. Lai and T. Tél, *Transient Chaos: Complex Dynamics on Finite Time Scales* (Springer, New York, 2011).

[67] X. Ni, L. Ying, Y.-C. Lai, Y. Do, and C. Grebogi, Phys. Rev. E **87**, 052911 (2013).

[68] A. N. Pisarchik and U. Feudel, Phys. Rep. **540**, 167 (2014).

[69] G.-L. Wang, H.-Y. Xu, and Y.-C. Lai, Sci. Rep. (2016).

[70] Z. Kovács, K. G. Szabó, and T. Tél, in *Nonlinearity and Chaos in Engineering Dynamics*, edited by J. M. T. Thompson and S. R. Bishop (John Wiley & Sons, Chichester, 1994), pp. 155–162.

[71] Y.-C. Lai, Phys. Lett. A **221**, 375 (1996).

[72] A. N. Pisarchik, Phys. Rev. E **64**, 046203 (2001).

[73] F. Prengel, A. Wacker, and E. Schöll, Phys. Rev. B **50**, 1705 (1994).

[74] N. G. Sun and G. P. Tsironis, Phys. Rev. B **51**, 11221 (1995).

[75] A. Amann, A. Wacker, L. L. Bonilla, and E. Schöll, Phys. Rev. E **63**, 066207 (2001).

[76] D. Huang, P. M. Alsing, T. Apostolova, and D. A. Cardimona, Phys. Rev. B **71**, 195205 (2005).

[77] D. Huang and P. M. Alsing, Phys. Rev. B **78**, 035206 (2008).

[78] D. Huang and D. A. Cardimona, Phys. Rev. B **67**, 245306 (2003).

[79] D. Huang, S. K. Lyo, and G. Gumbs, Phys. Rev. B **79**, 155308 (2009).

[80] E. Ott, *Chaos in Dynamical Systems*, 2nd ed. (Cambridge University Press, Cambridge, UK, 2002).

[81] Y. Bomze, R. Hey, H. T. Grahn, and S. W. Teitsworth, Phys. Rev. Lett. **109**, 026801 (2012).

[82] M. Alvaro, M. Carretero, and L. Bonilla, Europhys. Lett. **107**, 37002 (2014).

[83] J. P. Crutchfield, J. D. Farmer, and B. A. Huberman, Phys. Rep. **92**, 45 (1982).

[84] J. M. Deutsch, J. Phys. A Math. Gen. **18**, 1457 (1985).

[85] L. Yu, E. Ott, and Q. Chen, Phys. Rev. Lett. **65**, 2935 (1990).

[86] A. Hamm, T. Tél, and R. Graham, Phys. Lett. A **185**, 313 (1994).

[87] Y.-C. Lai, Z. Liu, L. Billings, and I. B. Schwartz, Phys. Rev. E **67**, 026210 (2003).

[88] T. Tél and Y.-C. Lai, Phys. Rev. E **81**, 056208 (2010).

[89] F. Bass and A. Tetervov, Phys. Rep. **140**, 237 (1986).

[90] A. A. Ignatov and Y. A. Romanov, Sov. Phys. Solid State **17**, 2216 (1975).

[91] A. A. Ignatov and Y. A. Romanov, Phys. Status Solidi B **73**, 327 (1976).

[92] V. V. Pavlovich and E. M. Epshtein, Sov. Phys. Semicond. **10**, 1196 (1976).

[93] A. A. Ignatov, E. Schomburg, J. Grenzer, K. Renk, and E. Dodin, Zeitschr. Phys. B Condens. Matter **98**, 187 (1995).

[94] P. K. Tien and J. P. Gordon, Phys. Rev. **129**, 647 (1963).

[95] G. Platero and R. Aguado, Phys. Rep. **395**, 1 (2004).